THE ASTROPHYSICAL JOURNAL, 473:781–796, 1996 December 20

X-RAY LINES IN ACTIVE GALACTIC NUCLEI AND PHOTOIONIZED GASES

HAGAI NETZER[1]
School of Physics and Astronomy and the Wise Observatory, The Beverly and Raymond Sackler Faculty of Exact Sciences, Tel Aviv University, Tel Aviv 69978, Israel
Received 1996 April 29; accepted 1996 July 11

ABSTRACT

This paper addresses the observed 0.1–10 keV spectrum in active galactic nuclei (AGNs) and other photoionized gases. Detailed calculations, encompassing a large range in density (10–10^{14} cm^{-3}), column density (10^{21}–$10^{23.5}$ cm^{-2}), and level of ionization (3 orders of magnitude in ionization parameter), are described and discussed. The results are presented as line intensity and three types of equivalent width over the entire range of physical conditions.

We identify the most likely conditions in the X-ray–absorbing gas in AGNs and argue that its temperature is below 2×10^5 K and that it is thermally stable. The strongest 0.1–10 keV lines, when observed against the central source continuum, have typical equivalent widths of 5–50 eV and are thus at the limit of present-day detection. The equivalent width can be significantly stronger when the line is observed against the absorbed continuum. Much larger equivalent widths, of 100–1000 eV, are expected when the central continuum is obscured, as in Seyfert 2 galaxies. The importance of line-continuum fluorescence diminishes with line optical depth, and we do not find this process to be important in warm AGN absorbers. The X-ray line intensities depend on the gas density, especially for very low ($N < 10^3$ cm^{-3}) and very high ($N > 10^{12}$ cm^{-3}) densities. They are also sensitive to the geometry and covering fraction.

We discuss the ultraviolet and extreme-ultraviolet spectrum and argue that the highly ionized gas contributes significantly to the observed intensity of Ne VIII λ774 and, in some cases, also to O VI λ1035. We confirm that observed ultraviolet absorption lines, in several AGNs, originate from gas with conditions similar to the X-ray–absorbing gas and show the expected column density and absorption equivalent width for the strongest species. If indeed the same physical component, wherever C IV λ1549 absorption is visible, we predict substantially greater absorption in the line O VI λ1035. None of the observed *Extreme Ultraviolet Explorer* lines in the spectrum of NGC 5548 are consistent with the ionized gas component, and there is no satisfactory model to explain these observations.

A new model is presented, in which evaporating "seeds" (high-density clouds or bloated stars) in the broad-line region are filling the intercloud medium with material that is streaming outward. The material's location, density, column density, covering fraction, and perhaps also dynamical state are consistent with observed properties of X-ray and ultraviolet absorbers.

Subject headings: galaxies: active — galaxies: ISM — galaxies: nuclei — line: formation — X-rays: galaxies

1. INTRODUCTION

Many quasars and other active galactic nuclei (AGNs) contain significant amounts of highly ionized material that substantially modifies the 0.1–10 keV spectrum. This X-ray component has been named the "ionized absorber" or "warm absorber" and has been studied in numerous papers (e.g., Halpern 1984; Pan, Stewart, & Pounds 1990; Turner & Pounds 1989; Yaqoob & Warwick 1991; Nandra & Pounds 1992, 1994; Fabian et al. 1994; Fiore et al. 1993; Mathur et al. 1994; Mathur, Elvis, & Wilkes 1995; George, Turner, & Netzer 1995; Reynolds et al. 1995). Theoretical studies of ionized absorbers include, among others, Halpern (1984), Krolik & Kallman (1984), Ferland & Rees (1988), Netzer (1993), Mathur et al. (1994), Netzer, Turner, & George (1994), Reynolds et al. (1995), George et al. (1995), Krolik & Kriss (1995), and Turner, Netzer, & George (1996). The most detailed theoretical studies are by Netzer (1993, hereafter Paper I) and by Krolik & Kriss (1995, hereafter KK95). These papers approached the problem from different viewpoints. While Paper I discussed the absorption, emission, and reflection of equilibrium gas, with emphasis on small dimensions and high densities, KK95 focused on low-density, more distant material and included a discussion on gas motion and stability.

This paper addresses the 0.1–10 keV emission-line spectrum in AGNs and other photoionized plasmas. It provides detailed calculations under a large range of density, column density, and ionization level and various geometries. Compton-thick media are not treated, and the reader is referred to George & Fabian (1991) and Życki et al. (1994) for information and other references. The results of the calculations are computed line intensities and equivalent widths that can be directly compared with the observations. We also compute the intensity of the strongest ultraviolet and extreme-ultraviolet emission lines and the equivalent widths of ultraviolet absorption lines claimed to have been associated with ionized X-ray absorbers (Mathur et al. 1995 and references therein). Section 2 explains the method and details of the calculation, and § 3 presents the results in various graphical forms. The discussion in § 4 compares the new calculations with AGN observations and suggests a new model that combines many of the observed emission

[1] Visiting scientist, Laboratory for High Energy Astrophysics, NASA Goddard Space Flight Center.

and absorption properties. More information about the calculations is given in the Appendix.

2. CALCULATIONS

2.1. *Method*

Our aim is to calculate the emergent 0.1–10 keV spectrum of gas that is exposed to a source of hard ionizing radiation. The premise is that X-ray observations with sufficient energy resolution will be compared with the results of the calculation and used to deduce the physical conditions in the gas, its location, and its distribution. The following spectral components are included: the incident continuum (bare or attenuated by absorption), the gas's intrinsic emission, and the scattered central continuum radiation. The general method and terminology follow Paper I, where most of the parameters are defined. Here we only give a brief summary of the model's more important ingredients.

We use a sophisticated photoionization code, ION, and a series of spectrum-combining routines, to calculate the spectrum and physical parameters of a gas in thermal and ionization equilibrium. The code incorporates full temperature and radiative transfer solutions and makes use of modern atomic data. All important excitation and ionization processes are included, and the emission, absorption, and reflection of the gas are calculated self-consistently. ION and its applications are described in Paper I, and several new features are detailed below and in the Appendix.

The model assumes a central, pointlike radiation source and an ensemble of "clouds" that are specified by their hydrogen density ($n_{\rm H}$), hydrogen column density ($N_{\rm col}$), chemical composition, and distance from the center (r). The first step treats a single cloud far enough from the source such that a thin-shell approximation can be used (but see comments about low-density models). The results are later combined into the ensemble spectrum in one of several geometries. The covering fraction of the system, C_f, is allowed to vary with the additional assumption that the clouds are either much smaller or much larger than the central source's size. Unless otherwise specified, all models discussed below assume small clouds.

The central source spectrum is typical of intermediate-luminosity AGNs. For simplicity, and for ease of reproduction, it is made of several power-law segments, each specified by its energy spectral index α ($F_\nu \propto \nu^{-\alpha}$). Important continuum characteristics are the total energy in the ultraviolet bump (1–100 eV), the slope of the 0.2–10 keV continuum, the ultraviolet (2500 Å) to X-ray (2 keV) slope, α_{OX}, and the infrared luminosity. Most models shown here assume α(0.2–50 keV) = 0.9, $\alpha_{OX} = 1.5$, and ultraviolet-to-optical energy slope of 0.5, extending from 0.12 to 3 ryd. We have also used the Krolik & Kriss continuum, which is defined in KK95 and has $\alpha_{OX} = 1.25$.

Regarding the infrared continuum, its exact spectral shape is important only in the high-density limit ($n_{\rm H} > 10^{11}$ cm^{-3}; see § 3.5), where it has a significant effect on the physical conditions in the ionized gas. It is not yet clear what fraction of the AGN infrared continuum is emitted by the central powerhouse and what is thermal emission due to reprocessing by dust (see, e.g., Laor 1990; Ward et al. 1987). Moreover, this fraction may be different in radio-loud and radio-quiet sources. Here we consider two possibilities: (1) a "weak IR continuum," in which there is a rise from 0.12 to 0.03 ryd, with an energy slope of 1.2, and a sharp drop at energies below 0.03 ryd, and (2) a "strong IR continuum," in which the central infrared source extends from 0.12 to 0.01 ryd, with a slope of 1.06, with a sharp drop beyond that. Both continua are far less luminous than most AGNs at far-infrared energies, in accord with the assumption that much of this emission originates in extended sources. The two continua are shown in Figure 1, and a discussion of the resulting electron temperature is given in § 3. The fiducial density chosen for this work is $n_{\rm H} = 10^{11}$ cm^{-3}, slightly larger than a typical broad-line region (BLR) density. At this density, the differences between the two continua are marginal. Unless otherwise specified, all results shown are for the "weak IR continuum."

A fundamental variable of the calculation is the ionization parameter, U. This name has been used loosely in the literature to define several different quantities. In Paper I, it was defined by the Lyman continuum photon flux per unit density, which is somewhat problematic since most of the photon flux is emitted in a part of the spectrum (the ultraviolet bump) that contributes only little to the ionization of the abundant 0.1–10 keV ions. Thus models with similar ionization parameters can differ substantially in their resulting X-ray ionization. We therefore introduce the X-ray ionization parameter, $U_{\rm X}$, which is defined in a similar fashion over the restricted 0.1–10 keV energy range,

$$U_{\rm X} \equiv \int_{\nu(0.1\ {\rm keV})}^{\nu(10\ {\rm keV})} \frac{L_\nu/h\nu}{4\pi r^2 n_{\rm H} c}\, d\nu\ , \qquad (1)$$

where L_ν is the monochromatic luminosity and c is the speed of light. The level of ionization of most X-ray–emitting species is directly proportional to $U_{\rm X}$, and typical values of interest are in the range 0.1–1. For the spectral shape chosen here (Fig. 1), the ratio of the traditional ionization parameter $U(>1$ ryd) (the one defined over the full

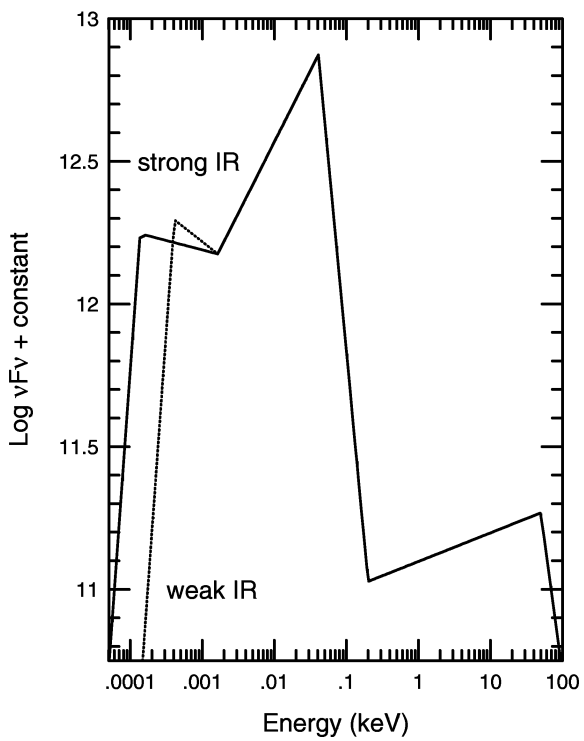

FIG. 1.—The two central continua considered in this work

Lyman continuum) and the one used here is $U(>1 \text{ ryd})/U_X = 141$. The ratio with $\xi \equiv L/nR^2$, used by KK95 and others, where L is the integrated 1–1000 ryd luminosity, is $\xi/U_X = 4.9 \times 10^3$.

All models calculated here assume undepleted "cosmic abundances," with (He, C, N, O, Ne, Mg, Si, S, Fe)/H = (1000, 3.7, 1.1, 8, 1.1, 0.37, 0.35, 0.16, 0.4) $\times 10^{-4}$. The chosen iron abundance is somewhat higher than the most recent solar determination but is still perhaps low, considering galactic nuclei. Constant density is assumed throughout to facilitate comparison with other calculations. Such an assumption is not necessarily less physical than the constant-pressure assumption in situations in which the sound-crossing time of a cloud ($\sim 10^9 T_e^{-1/2}$ s) is longer than the central flux variability time. Only time-independent equilibrium calculations are shown. For comments on the validity of these assumptions, see Netzer (1990), KK95, and § 4.

A major goal of this investigation is to cover the entire range of observed conditions in AGNs. We have therefore considered a very large range in density (1–10^{14} cm^{-3}), column density (10^{18}–10^{24} cm^{-2}), covering factor (0–1), and ionization parameter ($0.01 < U_X < 10$). The low-density limit is set by the assumed interstellar density and the high-density limit by uncertainties in the three-body recombination rate and the continuum transfer, in conditions approaching those of stellar atmospheres. The maximum column density is set by the cloud's Compton depth since ION does not fully solve the transfer of the scattered continuum radiation and cannot be trusted at Compton depths larger than about unity. As for the gas density, we note that dilution and geometric factors cannot always be neglected at the low-density limit, as, with the assumed large column density, the dimension of a single cloud can exceed its distance from the center. This is particularly important for cases in which the density drops with distance, such as the $n_H \propto r^{-2}$ case discussed by KK95. Fortunately, no known AGN ionized absorber violates these density and column density limits.

Many of the results presented below are for a so-called standard case, for which $n_H = 10^{11}$ cm^{-3}, $N_{col} = 10^{22.5}$ cm^{-2}, and $C_f = 1.0$.

2.2. *Physical Processes*

The calculated 0.1–10 keV spectral features include absorption lines and edges, collisionally excited emission lines, recombination lines, linelike features due to bound-free transitions at low temperatures, and the scattered central radiation. Important considerations are the number of ions and levels, the method of solving the statistical equilibrium equations in the presence of significant line opacity, the destruction of line photons by continuum opacity, and the treatment of atomic processes under high-density conditions. The reader is referred to Paper I and the Appendix for more information.

Several aspects of the calculations require some explanation. First, the presence of Fe L-shell lines is known to be very important in X-ray plasmas (see, e.g., Liedahl, Osterheld, & Williams 1995). Most relevant for the present work are radiative and dielectronic recombination lines of Fe XVII–XXIII that result in broad emission features between 0.7 and 1.2 keV. The accurate calculation of such features is at the forefront of atomic physics, and the full set of atomic data was not available to us. Instead, we have taken the more limited approach of treating only the three to five strongest Fe L lines of each of the relevant ions and estimated, from their strength, the remaining contribution. The atomic data were kindly provided by D. Liedahl.

A potentially important process, in cases of obscured central continua, is absorption of continuum photons in bound-bound transitions, mostly by resonance lines. This process is commonly referred to as "continuum fluorescence" although other names have been used. KK95, following Band et al. (1990), extensively discussed this process and referred to it as "resonance-line scattering." They further claimed that it can considerably change the observed intensity of emission lines and can contribute significantly to the observed flux over parts of the spectrum, e.g., the 1–1.5 keV range.

It is easy to show that, for all models considered here, the contribution of continuum fluorescence to the intensity of strong emission lines is smaller than, or, at most, comparable to, the recombination contribution. This follows from the fact that the f-values of the strongest resonance lines, f_{ij}, and the corresponding continuum f-value, $f_c = \int_{\nu_0}^{\infty} (df/d\nu) d\nu$, where ν_0 is the ionization-edge frequency, are related. For many ions, $f_{ij} \simeq f_c$. Thus, for a line with frequency ν_l, the absorption cross section integrated over the line profile and the one integrated over the ground-level ionization continuum are comparable. Since most recombinations lead to line emission, we find that, for optically thin lines and continuum (where continuum fluorescence is most efficient), the relative number of line photons produced by the two processes is

$$\frac{N(\text{continuum fluorescence lines})}{N(\text{recombination lines})} = \frac{(\nu_l/\nu_o)^{-(\alpha+1)}(\pi e^2/mc) f_{ij}}{\int_{\nu_0}^{\infty} (\nu/\nu_0)^{-(\alpha+1)} a_\nu \, d\nu} \simeq \frac{3+\alpha}{2} \left(\frac{\nu_l}{\nu_0}\right)^{-(\alpha+1)}, \quad (2)$$

where the numerical factor was obtained from integrating over the continuum and the absorption cross section. Thus the number of photons absorbed by optically thin resonance lines is of the same order as the number of photons produced by recombination.

The above ratio for H-like and He-like ions, for a typical $\alpha \simeq 1$ continuum, is of order 3.5, and more accurate calculations may deviate from this expression by a small amount. For example, at the optically thin, low-density limit, the ratio for H-like ions is larger than in equation (2) since less than 50% of all ionizations result in Lyα emission. Also, there are cases in which the line is much removed from the ionization edge and the ratio is larger than 3.5. Notable examples are the strong $2s$–$2p$ Li isoelectronic sequence lines, like O VI λ1035, and lines like Fe XV λ284. Finally, the above ratio is *independent* of the line width.

At a certain depth into the cloud, where the line optical depth is τ_{in} and the mean continuum optical depth is τ_c, the above ratio should be multiplied by an additional factor of $\epsilon(\tau_{in})/e^{-\tau_c}$, where $\epsilon(\tau_{in})$ is the one-sided escape probability for the line. This factor is much smaller than unity for all $\tau_{in} \gg 1$. Thus recombination dominates at all cases of significant line opacity. In almost all models considered here, most resonance lines are optically thick even if large microturbulence is assumed. Thus continuum fluorescence is considerably less important than in optically thin cases. The lines are optically thin, and continuum fluorescence more

efficient, when the gas column density is small. These are precisely the cases in which line emission is insignificant because of the small emission measure.

There are some important deviations from the above general scheme. The ionizing photons may be absorbed by other ions or elements while the absorption lines, with their lower energy, need not be affected as much. A well-known example is the Fe II spectrum of AGNs, in which hundreds of ultraviolet lines are capable of absorbing a sizable fraction of the ultraviolet continuum (Wills, Netzer, & Wills 1985 and references therein) while no ionization of Fe^+ takes place since hydrogen is mostly neutral. A somewhat similar case pertaining to the X-ray spectrum is the absorption of Fe L line photons. The ionization potential of iron ions with 10 or fewer electrons covers a small energy range (1266–2045 eV) over which some or all ions compete for the same ionizing photons. Thus the radiation absorbed by each iron ion is only a fraction of the total available radiation while the absorption lines are exposed to the full continuum flux. Under such conditions, continuum fluorescence can dominate over recombination in producing emission-line photons. As explained, only a subsample of all Fe L lines are included in the present work, and because of this, the computations underestimate the Fe L line intensities.

Finally, we note again that the contribution of continuum fluorescence to the observed emission lines is only important if the central continuum is obscured or if the line of sight to the center does not pass through the ionized gas. In all other cases, the absorption and emission contributions due to this process almost identically cancel out. Bulk velocity can shift the absorption component relative to the emission, in which case both components will be observed. Such models have not been calculated.

ION includes a complete treatment of the continuum fluorescence process for all resonance lines. This amounts, for a two-level system, to solving the following rate equation:

$$\frac{dn_2}{dt} = -\epsilon_{12} A_{21} n_2 - \epsilon(\tau_{\rm in}) A_{21} \frac{c^2 L_\nu}{32 h \nu^3 \pi^2 r^2} \left(n_2 - \frac{g_2 n_1}{g_1} \right), \tag{3}$$

where ϵ_{12} is the full (two-sided) local escape probability and we have neglected other excitation processes (Elitzur & Netzer 1985; Netzer 1990). Most calculations assume thermal motion for all ions, but we have tried several cases with large microturbulent velocities (see example in § 3). The continuum fluorescence of iron Kα lines, except for the He-like and H-like iron, is not significant for the column density considered here because of the efficient Auger destruction. The detailed calculations confirm the general estimate that continuum fluorescence is of little significance under almost all conditions considered here. A few lines in a few models are increased by a factor of order 2, and these are not the strongest 0.1–10 keV lines.

Related to the above discussion are X-ray absorption lines. Such lines were mentioned by KK95, and others, as important for the determination of absorption-edge energies next to strong transitions. Our calculations do not show strong absorption lines even for turbulences significantly larger than the thermal line widths. This is mostly due to the fact that such features would almost disappear in large covering factor geometries. We note, however, that our line list is not identical to the one used by KK95, and some of the differences may be due to this.

3. RESULTS

3.1. *Electron Temperature*

The electron temperature depends on the shape of the ionizing continuum, the gas density, chemical composition, and ionization parameter. The dependece on ionization parameter is shown in Figure 2 for the standard continuum and chemical composition, as a T_e versus $\log (U_{\rm X}/T_e)$ diagram. It illustrates the range of expected temperature, as well as the region of thermal stability (see, e.g., Krolik, McKee, & Tarter 1981). As evident from the diagram, the gas is thermally stable for all temperatures below about 2.2×10^5 K, much higher than customarily assumed.

The issue of gas stability has recently been addressed by Marshall et al. (1993), KK95, and Hamann et al. (1995a). The Marshall et al. calculations show that the onset of instability depends on the metallicity, opacity, and continuum shape. To further investigate the maximum temperature for a stable solution, $T_{\rm max}$, we have calculated several models with different X-ray slope α(0.2–50 keV). The models assume the same metallicity and general broken power-law continuum of Figure 1, and the change of slope is obtained by fixing the 0.2 keV point and changing the 50 keV flux. This changes α_{OX}, but the effect on $T_{\rm max}$ is negligible. Representative values are given in Table 1.

As evident from the table, $T_{\rm max}$ covers the range (0.7–3.3) $\times 10^5$ K, with larger $T_{\rm max}$ corresponding to steeper con-

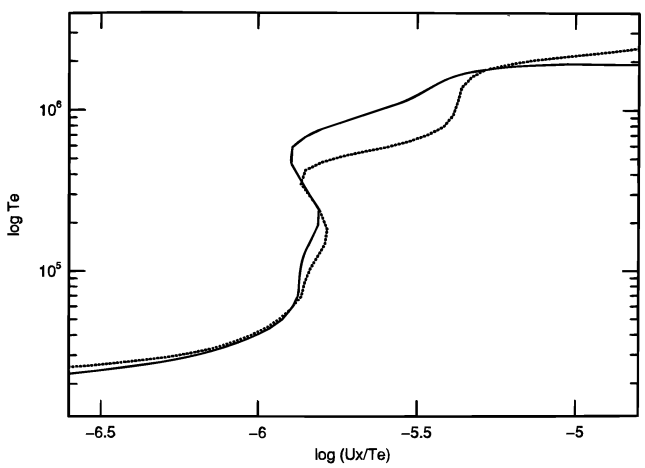

FIG. 2.—Electron temperature as a function of $U_{\rm X}/T_e$ for two densities, $N = 10^{11}$ cm^{-3} (*solid line*) and $N = 10^4$ cm^{-3} (*dotted line*).

TABLE 1

MAXIMUM STABLE SOLUTION TEMPERATURE AND CORRESPONDING IONIZATION PARAMETER AND LEVEL OF IONIZATION OF OXYGEN FOR SEVERAL CONTINUA

α(0.2–50 keV)	$T_{\rm max}$ (K)	$U_{\rm X}$	O^{+6}/O	O^{+7}/O
0.5	6.1×10^4	0.06	0.45	0.43
0.7	1.7×10^5	0.22	0.07	0.42
0.9	2.2×10^5	0.39	0.03	0.32
1.1	2.4×10^5	0.65	0.02	0.26
1.3	2.7×10^5	1.08	0.01	0.21
1.5	3.3×10^5	2.08	0.004	0.14

tinua and larger U_X. Also shown are the fractional abundance of O^{+6} and O^{+7} at the ionization parameter corresponding to T_{max}. Both ions are abundant enough, in all cases, to produce significant absorption edges. At this U_X, O^{+7} is more abundant than O^{+6}, thus at slightly smaller U_X, we expect a comparable amount of absorption by the two ions. Since most observed warm AGN absorbers show both O^{+6} and O^{+7} absorption edges, we expect their temperature to be slightly below T_{max}. Thus the absorbing gas is probably thermally stable. This has important consequences for the physics and location of the absorbing gas, as discussed in § 4.

The X-ray–ionized gas need not be in thermal and radiative equilibrium (KK95). We proceed to discuss a large range of models, including some with very large U_X, in which the temperature exceeds T_{max}. The implications are discussed in § 4.

3.2. *Line Intensity and Equivalent Width*

All calculations in this paper assume isotropic scattering and emission of line and continuum photons.

A convenient way of expressing the calculated intensities is relative to the H-like O VIII 653 eV line, which is always among the strongest in the spectrum. Alternatively, we can specify the line equivalent width (EW) in units of the local continuum. Three different types of EW can be defined:

1. *Relative to the incident continuum*, EW(con).—This EW is measured relative to the unattenuated central continuum. It is rarely observed, because of absorption and the locally produced emission, but is a convenient way to compare different lines.

2. *Relative to the observed continuum*, EW(obs).—This is the measured equivalent width, which depends on the continuum luminosity and attenuation, the local line and continuum radiation, and the reflection of the central continuum radiation. Note again that the calculations assume the same energy for absorption and emission lines, i.e., no net radial motion.

3. *Relative to the gas continuum*, EW(gas).—In some cases, like in Seyfert 2 galaxies, the central continuum is obscured by an X-ray–opaque component, e.g., a dusty torus. In this case, the emission-line equivalent width is measured against the local (free-free, bound-free, and scattered central source) continuum. Normally, EW(gas) is larger than EW(con) and EW(obs).

Consider first EW(con) for the comparison line O VIII 653 eV. Assume steady state photoionized gas, in which the electron temperature is much lower than the equilibrium plasma temperature and almost all oxygen is either O^{+7} or O^{+8}. The maximum number of oxygen ionizations is found by counting all $E > 871$ eV photons, and the intensity of the O VIII 653 eV line is readily obtained since a known fraction of all O^{+8} recombinations (60%–100%, depending on the density and line optical depth) result in line photons. For example, the maximum EW(con) for the Figure 1 continuum is approximately 530 eV. Such a strong line is never observed, for several reasons. First, the absorption of all $E > 871$ eV photons requires a substantial high-energy opacity, which leads to a region where O^{+6} and other oxygen ions are also abundant. Thus some $E > 871$ eV photons are absorbed by oxygen ions other than O^{+7}. Second, far from the 871 eV threshold, other abundant ions, such as highly ionized neon, magnesium, and iron, strongly compete with oxygen for the absorption of ionizing photons. For a solar-composition gas, very few of the $E > 2$ keV photons are absorbed by oxygen. Third, large O^{+6} and O^{+7} columns are normally associated with large C^{+5} and N^{+6} columns, capable of absorbing the emitted O VIII 653 eV line. The combined effect of all three is to reduce significantly the EW(con) of the line. As shown below, the largest calculated EW(con) for the line is less than 20% of the above theoretical maximum. Since the O VIII 653 eV line is always among the strongest in the spectrum, it is easy to see why in photoionized gases EW(obs) hardly ever exceeds a few tens of eV.

3.3. *Ionization Parameter*

Line intensities as functions of U_X, relative to the O VIII 653 eV line, are shown in Figure 3. Here the density, column density, and covering fraction are all at their standard values: $n_H = 10^{11}$ cm^{-3}, $N_{col} = 10^{22.5}$ cm^{-2}, and $C_f = 1$. As expected, O VIII 653 eV, C VI 364 eV, and O VII 568 eV are the strongest low-ionization lines. Lines of Mg, Si, and S dominate at larger U_X, and He-like iron is strong in the extreme-ionization range. Several L-shell Fe lines are strong too (725, 775, and 885 eV) but not as strong as the oxygen and neon lines.

The equivalent widths of these lines are shown in Figure 4. As explained, EW(con) is a measure of the line production efficiency and the line destruction. EW(obs), however, is very sensitive to the presence of absorption, especially at low ionization parameters. This is very important for all lines between about 1 and 2 keV (Ne X 1.02 keV, Mg XI 1.34 keV, Mg XII 1.47 keV, Si XIII 1.85 keV), where a smoothly attenuated continuum is often observed. In such cases, the lines are observed against a suppressed continuum, and EW(obs) can exceed 100 eV. This is also evident in Figure 5, where we show calculated spectra for several values of U_X. For example, Ne IX 915 eV, which is never the strongest line in the spectrum, can attain very large values of EW(obs) since its energy is close to the energy of maximum soft X-ray absorption.

3.4. *Column Density*

A large column density model is characterized by a wide range of ionization stages and a lower mean electron temperature. A small column density model is more uniform, with fewer strong emission lines of similar levels of ionization. Figure 6 shows three-dimensional plots for several strong emission lines as functions of U_X and column density, all for the case of $C_f = 1.0$ and $n_H = 10^{11}$ cm^{-3}. The increase in EW(con) with increasing column density, which reflects the increased efficiency of absorbing the ionizing radiation, is evident in all cases. As explained, there is a natural limit to this process and a maximum value of EW(con). We also demonstrate in Figure 6 a case of a very large EW(obs) for a line (Si XIII 1.85 keV) whose energy is in the aforementioned 1–2 keV range, where continuum attenuation can cause a large contrast in flux between the line and the adjacent continuum.

3.5. *Gas Density*

Most of the important physical processes are density sensitive. As the gas density increases, the high-temperature dielectronic recombination rate is reduced, three-body recombination increases, and free-free heating can considerably change the heating-cooling budget of the gas.

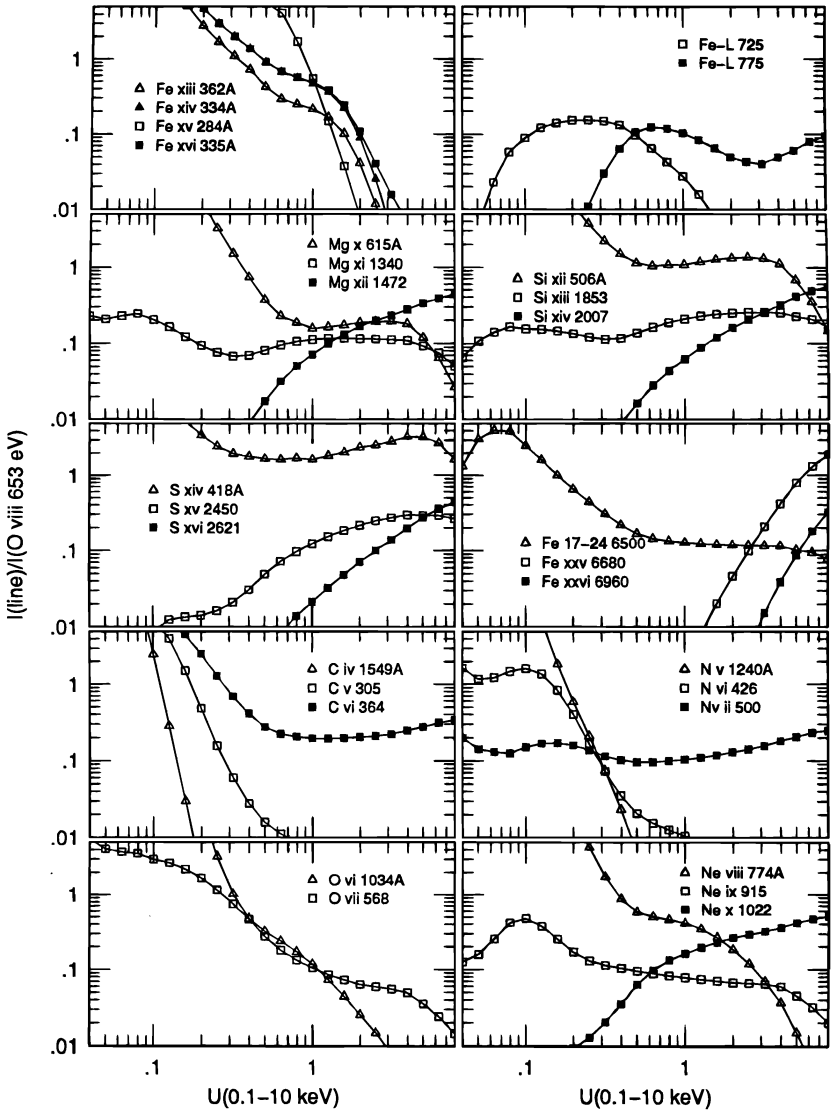

FIG. 3.—Line ratios, relative to O VIII 653 eV, of the strongest emission lines

Figure 7 shows the volume-averaged electron temperature as a function of density for the canonical model of $N_{\rm col} = 10^{22.5}$ cm^{-2}, $C_f = 1$, and $U_{\rm X} = 0.2$ over a range of densities. The diagram is meant to illustrate the dependence of temperature on physical conditions and not to suggest a realistic model for AGNs (the clouds are obviously too close to the center for the highest density considered). There are two temperature curves, one for the case of "strong IR" continuum and one for the "weak IR" continuum (§ 2 and Fig. 1). Increasing the density at low densities influences the temperature because of the collisional suppression of several important coolants, such as the Ne V fine-structure lines. A more profound effect occurs at $n_{\rm H} > 10^{11}$ cm^{-3}. At this limit, the large increase in temperature is caused by the collisional suppression of several important coolants (mostly semiforbidden lines) and by free-free heating, which becomes a significant heating source for the gas. The latter is evident from the marked difference between the two types of continua, where the one emitting more infrared flux results in a significantly higher temperature.

The increased gas density results in some complicated changes in line EWs, as demonstrated in Figure 8. At low densities, the main effect is due to changes in ionization caused by the changing temperature. This affects the line intensities directly (change in temperature) and indirectly (change in opacity and line destruction). At intermediate and high densities, where the temperature is almost constant, the change in the level of ionization is due to the collisional suppression of dielectronic recombination (see Appendix). At very high densities, the rising temperature, and the onset of fast three-body recombination, causes more ionization changes, as well as nonnegligible collisional contribution to lines of carbon, nitrogen, and oxygen. Finally, collisional mixing of the $2s$ and $2p$ levels of H-like ions, mostly due to proton impacts (Zygelman & Dalgarno 1987), becomes significant at a density of about $1.8 \times 10^4 Z^{9.3}$, where Z is the atomic charge. Below the critical density for the process, some 30%–40% of all recombinations result in a two-photon continuum while, above this density, collisional mixing of the $n = 2$ levels weakens the two-photon emission and strengthens Lα by approximately 50%. The large increase in the equivalent width of O VIII 653 eV at around $n_{\rm H} = 10^{12}$ cm^{-3} is due to this process.

Finally, some of the so-called coronal lines are significant coolants under low-density, high-ionization conditions. For the typical $U_{\rm X} = 0.1$ model, their intensity is insignificant, but at somewhat lower ionization they are likely to be strong. The strongest expected lines are [Ne VI] 7.6 μm,

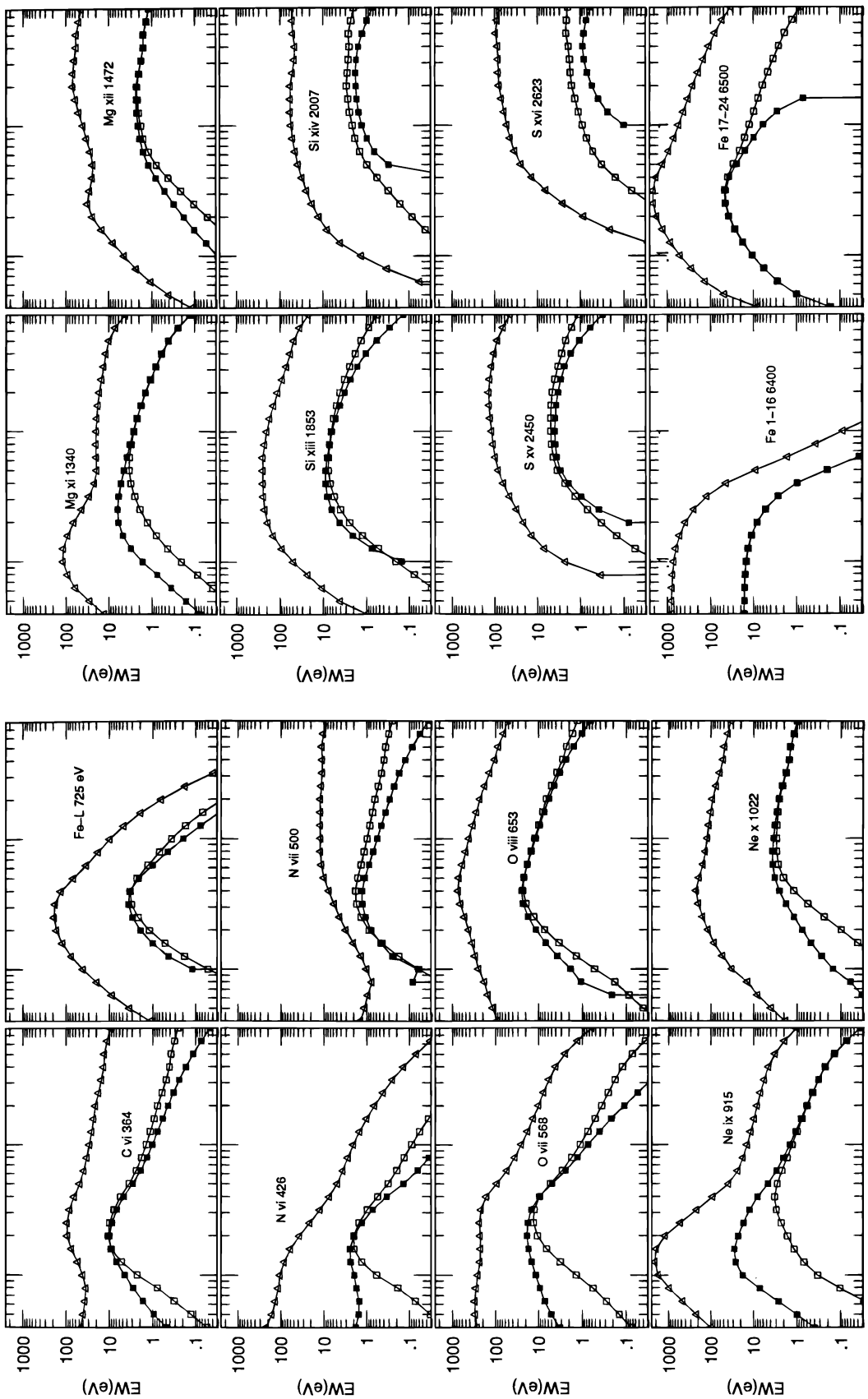

FIG. 4.—Calculated equivalent widths for several X-ray lines: EW(con) (*open squares*), EW(obs) (*filled squares*), and EW(gas) (*triangles*). The iron line equivalent widths include both Kα and Kβ.

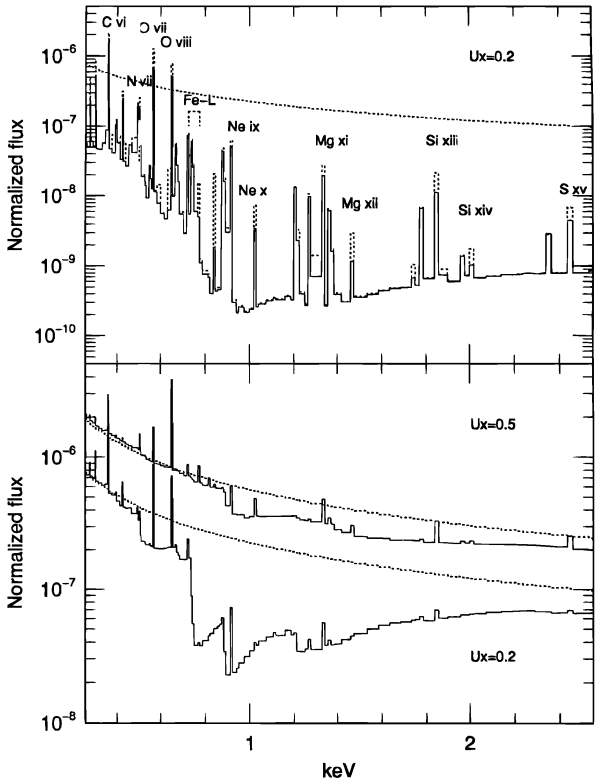

FIG. 5.—*Bottom*: Calculated spectra for two values of U_X, assuming thermal line widths. The dotted lines are the incident continuum, and the height of the emission lines is fixed by assuming an observed line width of 4000 km s^{-1}. *Top*: The $U_X = 0.2$ spectrum as seen for a case in which the central continuum is obscured. The dotted line is the same model with assumed microturbulent velocity of 300 km s^{-1}. Note the different vertical scales of the bottom and top panels.

[Fe X] λ6734, [Fe XIV] λ7891, and [Fe XIV] λ5303. The small observed equivalent width of such lines sets a limit on the amount of low-density, warm absorbing gas.

3.6. *Covering Fraction*

As discussed in Paper I and in § 2, the emergent line flux depends on both the local emissivity and the line absorption on the way out. The first reflects the local physical conditions and the second the overall geometry, which can be complicated and different for various lines of sight. For negligible continuous opacity, the line flux and EW(con) increase linearly with C_f. For large opacity, the observed equivalent widths are complicated functions of C_f. Under the simplest assumption of a thin spherical shell, we expect the maximum EW(con) for lines that are strongly absorbed by the continuum opacity to occur at $C_f \sim 0.5$ (Paper I). Obviously, this description is somewhat simplified since the increasing C_f also affects the ionization due to the interaction of lines and diffuse radiation with the gas.

Figure 9 demonstrates some of these possibilities. It shows calculated equivalent widths, as a function of C_f, for three of the strongest emission lines. The first case (Fig. 9*a*) is computed for O VIII 653 eV and Ne IX 915 eV. As evident from the diagram, the equivalent width of the two lines increases with C_f, but not in a linear way. Thus the full-coverage intensity of O VIII 653 eV is about 60% of the intensity it would have without absorption by other clouds. Ne IX 915 eV is even more heavily attenuated because of the larger opacity at 915 eV. Its full-coverage emergent flux is about 30% of the maximum it would have without the absorption. The maximum equivalent width for the two lines occurs at $C_f = 0.7$.

Figure 9*c* illustrates the covering-fraction dependence of O VII 568 eV and O VIII 653 eV in a low-density ($\langle n_H \rangle = 10^3$ cm^{-3}), $U_X = 0.24$ model similar to KK95 model *b*. It was calculated with the KK95 continuum, but the physical parameters are not identical since our temperature solution for a given flux is somewhat different from that of KK95. The temperature at the illuminated face is 3×10^5 K, and the dilution of the radiation field is negligible. The temperature across the gas in this model is not constant, because of the buildup of significant X-ray opacity. This reduces the emergent line flux. The peak EW(con) for O VIII 653 eV is at $C_f = 0.6$, close to the analytical estimate of 0.5, and the drop at larger C_f is due to continuum destruction of the lines. The theoretical (no absorption) linear increase of EW(con) with C_f is shown for comparison. Calculations like those of KK95 are expected to follow this linear curve and overestimate the line intensity at large C_f.

Line absorption by continuum opacity is not unique to large-C_f geometries. It occurs also in small covering fraction cases in which the line of sight to the source passes through clouds (e.g., a double-cone geometry with a line of sight passing through the cone). Lines whose intensity is significantly affected by continuum fluorescence (§ 2.2) will show more absorption than emission in such cases.

Finally, EW(gas), the line equivalent width for a completely obscured central source, depends only little on the geometry and C_f since the line flux and the continuum (diffuse emission and reflection), against which it is measured, are affected in a similar way by continuum opacity. This is illustrated in Figure 9*b*. There are small deviations from this scheme at large C_f since the level of ionization depends on the fraction of line and diffuse radiation that interacts with the gas.

4. DISCUSSION

While most of the previous results are quite general, the present section applies mostly to AGNs.

4.1. *X-Ray Absorption*

There are several published, detailed models of ionized X-ray absorbers, and it is interesting to note that those applied to the higher resolution observations (e.g., Reynolds et al. 1995; Weaver et al. 1994; George et al. 1995; Kriss et al. 1996b) seem to converge on a small range of ionization parameter, $U_X \simeq 0.1$–1. While a detailed comparison between the present work and the previous models is tricky, because of the different assumptions about the ultraviolet continuum, it is obvious that much higher or much lower ionization parameters are excluded. As shown earlier, this U_X corresponds to a thermally stable gas (Fig. 2 and Table 1). Thus it is likely that the observed ionized gas is in thermal equilibrium and that any unstable, larger U_X component is either absent or else totally transparent over the 0.1–10 keV range. Below we present a new model that makes use of this finding.

4.2. *X-Ray Emission*

The new calculations of the strong 0.1–10 keV emission lines will be useful for comparison with future X-ray observations. We have shown that if the central ionizing source is not obscured, the equivalent width of the strongest soft

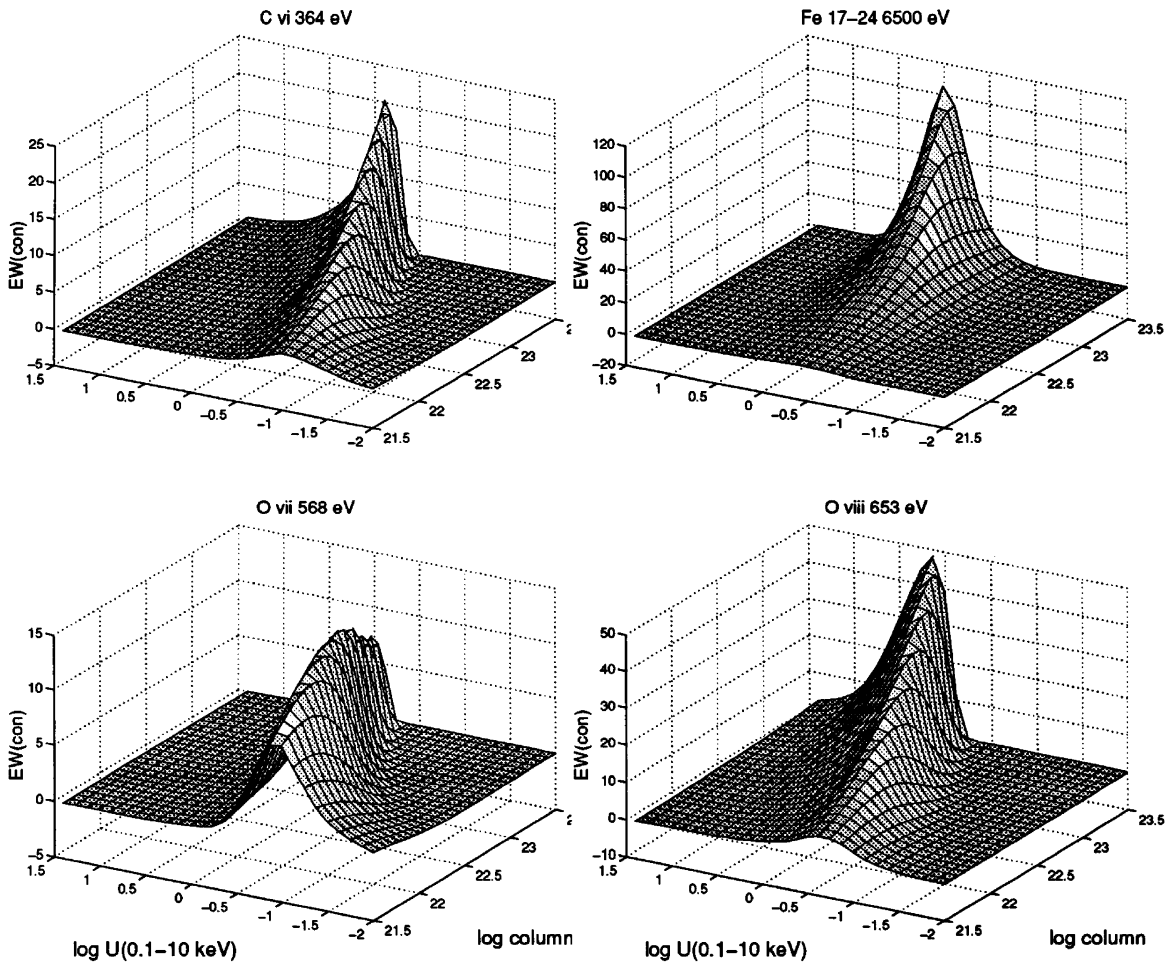

FIG. 6a

FIG. 6.—Three-dimensional equivalent width plots for strong X-ray lines. For Si XIII 1.85 keV, we show both EW(con) and EW(obs).

X-ray lines is predicted to be about 50 eV, with more typical values of about 10 eV. Larger equivalent widths are expected in regions of the spectrum in which the lines are observed against the attenuated central continuum. Notable examples are H-like and He-like lines of neon, magnesium, and silicon. Observations of several such lines (albeit with large uncertainties) have been reported in NGC 3783 (George et al. 1995) and NGC 4151 (e.g., Yaqoob et al. 1996), all at the limit of *ASCA*'s capability. Future X-ray experiments, with their much improved energy resolution, should have no difficulty detecting these lines.

X-ray emission lines with much larger equivalent widths are expected in cases in which the central continuum is totally obscured. The nuclei of Seyfert 2 galaxies that contain enough ionized material, like NGC 1068 (see, e.g., Marshall et al. 1993), are the best cases for comparison with the model predictions. Our calculations show that the line equivalent width, in such cases, is practically independent of the covering factor, so future detection is merely a question of adequate signal-to-noise ratio (S/N). We have also shown that at very low densities, the temperature and level of ionization of the gas may be unfavorable for the formation of the lines (e.g., Fig. 8). We could not compare our calculated EW(gas) to those of KK95, who aimed at similar physical situations, since those authors did not provide their result in a numerical form.

4.3. *UV and EUV Emission Lines*

Following the general discussion of Paper I, we have calculated the intensity and equivalent width of many UV emission lines. Only two of those, O VI λ1035 and Ne VIII λ774, are strong enough to be observed. Their calculated equivalent widths are shown in Figure 10 for the case of $n_{\rm H} = 10^{11}$ cm^{-3}, $C_f = 1$, and the full range of $U_{\rm X}$ and column density. The maximum calculated EW(obs) are 6 and 60 Å for Ne VIII λ774 and O VI λ1035, respectively.

O VI λ1035 is one of the strongest observed AGN lines, with rest equivalent width in the range 5–50 Å. Present BLR models are quite successful in predicting its intensity for "standard BLR" conditions with $C_f = 0.1$. Under favorable conditions, the contribution of highly ionized, $U_{\rm X} = 0.1$, gas to the line equivalent width is approximately $5C_f$ Å for $N_{\rm col} = 10^{22.5}$ cm^{-2}. The contribution is much smaller for larger $U_{\rm X}$. Thus a full-coverage warm absorber can substantially contribute to the observed intensity in objects of relatively weak O VI λ1035. We note, however, that O VI λ1035 is stronger in low-luminosity AGNs, where warm absorbers seem to be more common. The idea of a large contribution to O VI λ1035 from an optically thin component is not new (Netzer 1976) and has been studied in detail by Shields, Ferland, & Peterson (1995). Here we have demonstrated that the ionization parameter of this com-

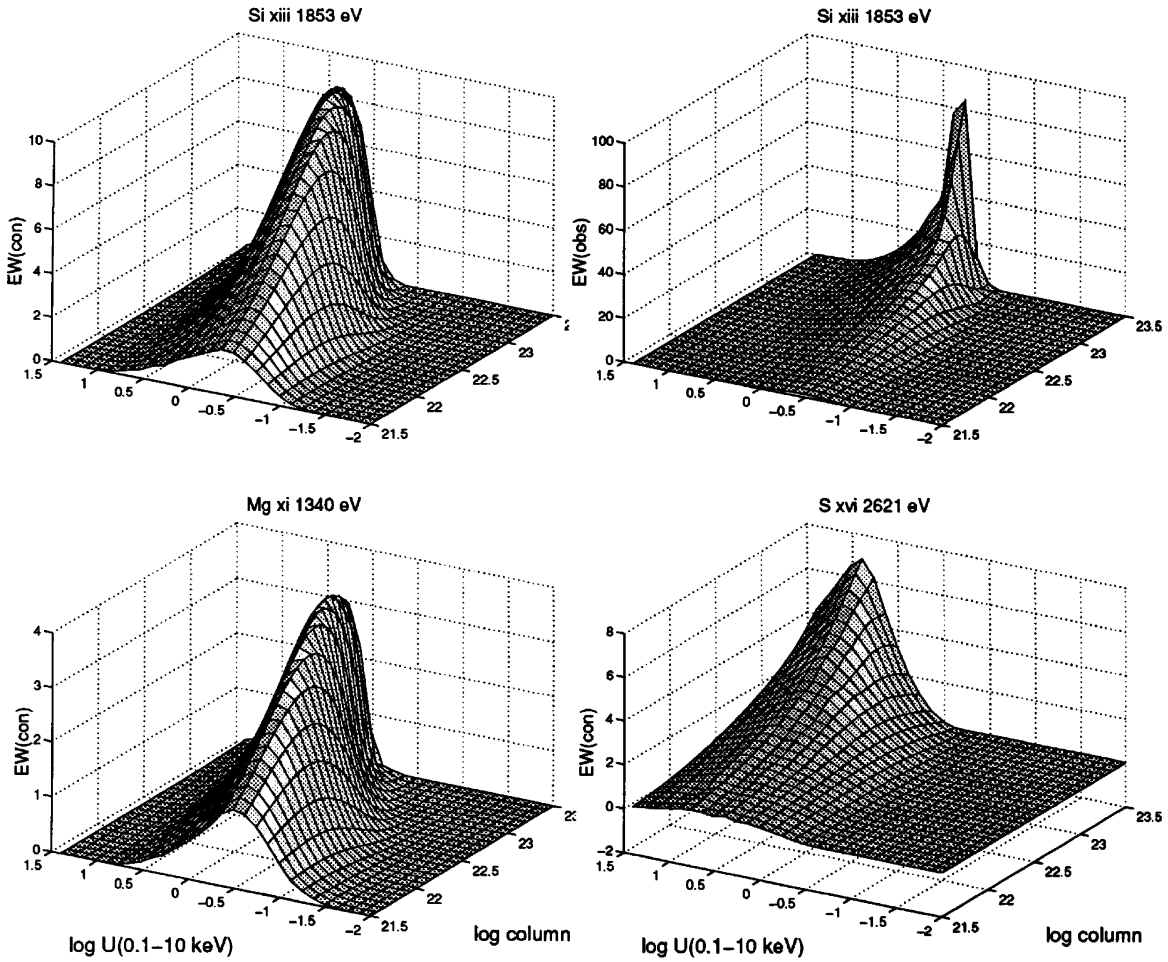

FIG. 6b

ponent is considerably higher than previously thought. We note, however, a large uncertainty in the calculated intensity of the line due to the unknown continuum shape around 120 eV.

As for Ne VIII λ774, the line is calculated to be strongest for $U_X \simeq 0.15$ with maximum, full-coverage equivalent width of about 3 Å for a column density of $10^{22.5}$ cm^{-2} and about 6 Å for a column density of $10^{23.5}$ cm^{-2}. This line has recently been observed in several *Hubble Space Telescope* Faint Object Spectrograph snapshot observations (Hamann, Zou, & Tytler 1995b) and in the quasar PG 1148+549 (Hamann et al. 1995a) with typical rest equivalent width of 5–10 Å. Thus a warm absorber with properties

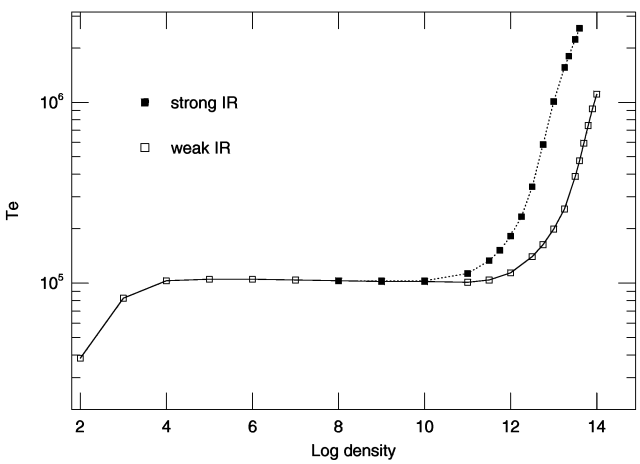

FIG. 7.—Electron temperature as a function of density for the standard case with $U_X = 0.2$ and two assumptions about the shape of the central continuum, as marked. Note the larger temperature increase in the "strong IR" continuum, due to free-free heating.

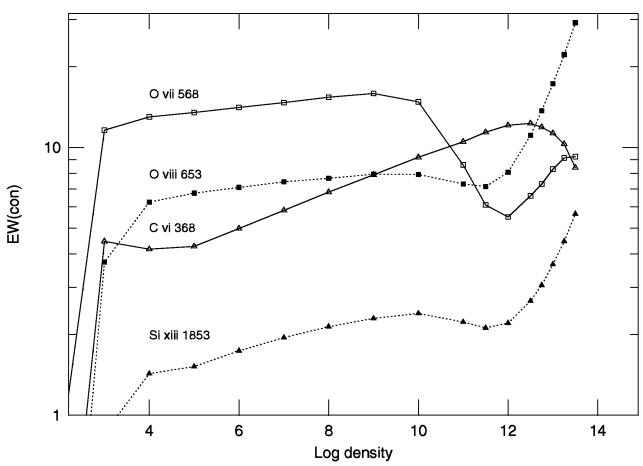

FIG. 8.—EW(con) as a function of density for several lines. $U_X = 0.2$, $N_{col} = 10^{22.5}$ cm^{-2}, and $C_f = 1.0$.

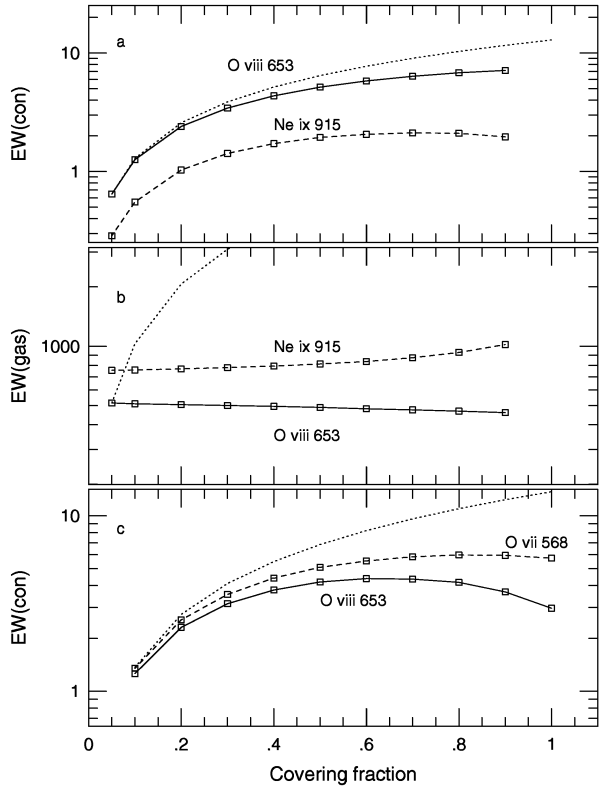

FIG. 9.—(*a*) EW(con) and (*b*) EW(gas) as functions of covering fraction for the standard case with $U_X = 0.2$ and $N_{col} = 10^{22.5}$ cm^{-2}, and (*c*) change of EW(con) with C_f for a case similar to KK95 model *b*. Dotted lines in all diagrams indicate the predicted linear increase of EW(con) and EW(gas) with C_f for the O VIII 653 eV line.

similar to those discussed here can explain a large fraction of its observed intensity provided that the covering fraction is close to unity. Hamann et al. (1995a) have investigated this issue and reached similar conclusions. Their model, while different from ours in details, produces similar results, and we agree with most of their conclusions.

Finally, we do not show the calculated EW of other UV lines that are either too weak (C IV λ1549 and N V λ1240) or else too far into the UV to be observed (Mg X λ615 and Si XII λ506).

Regarding the EUV range, the only published results are by Kaastra, Roos, & Mewe (1995), who observed NGC 5548 with the *Extreme Ultraviolet Explorer* (*EUVE*) satellite. These authors obtained a reasonable S/N spectrum of the 70–100 Å range and claimed to have detected several emission lines at 72 Å, 90 Å, and perhaps also 85 Å. The proposed line identifications are Ne VII λ88, Ne VIII λ88, and Si VII λ70.

Our calculations show that the strongest 70–100 Å emission lines in photoionized gas are due to recombination. These lines are the Hβ transition of O^{+8}, Ne VII λ88, and Ne VIII λ88. Some collisionally excited Fe XVIII lines are strong too. The neon-line intensities can be compared with the intensity of Ne VIII λ774. This yields

$$\frac{I(\text{Ne VII } \lambda 88)}{I(\text{Ne VIII } \lambda 774)} \simeq \frac{5 \times 10^{-4} T_e^{-0.3}}{\exp\left(-1.86 \times 10^5 / T_e\right)}, \quad (4)$$

$$\frac{I(\text{Ne VIII } \lambda 88)}{I(\text{Ne VIII } \lambda 774)} \simeq \frac{10^{-3} T_e^{-0.3}}{\exp\left(-1.86 \times 10^5 / T_e\right)} \frac{N(\text{Ne}^{+8})}{N(\text{Ne}^{+7})}, \quad (5)$$

where we have assumed that some 20% of all recombinations of Ne^{+6} and Ne^{+7} lead to the above recombination lines. At the typical electron temperature of $\sim 10^5$ K, both recombination lines are orders of magnitude weaker than Ne VIII λ774.

Our calculations show also that the equivalent width of the stronger neon recombination line, Ne VIII λ88, assuming thermal line widths, is only 0.3 Å, much weaker than observed by Kaastra et al. (1995). The ratio with Ne VIII λ774, for these maximum-intensity conditions ($U_X = 0.26$, $N_{col} = 10^{23.5}$), is 7×10^{-4} (!). Moreover, for the conditions most favorable to the production of the above neon lines, their total flux is only a few percent of the hydrogen Lyα flux originating in the same clouds. If the line fluxes are as large as claimed, the Lyα flux would exceed the observed value by a very large factor, i.e., the observed Lyα in this source would have to originate from the highly ionized component. This is definitely not the case in NGC 5548.

Kaastra et al. (1995) have noted the expected weakness of the neon recombination lines and suggested that continuum fluorescence, under large-microturbulence conditions, can explain the discrepancy. We have tested this idea, under a very large range of velocities, by using our detailed calcu-

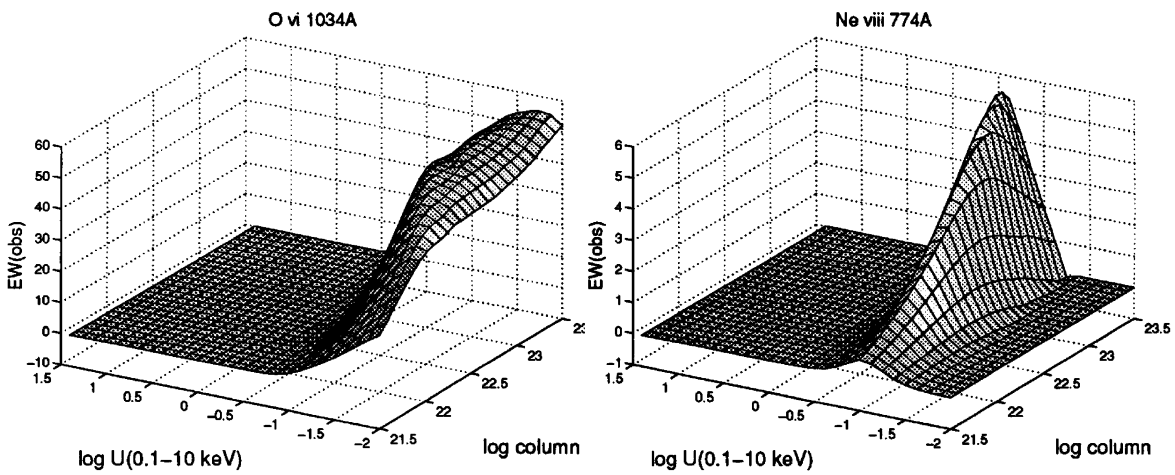

FIG. 10.—Three-dimensional observed equivalent widths for Ne VIII λ774 and O VI λ1035

lations and assuming no line-of-sight absorption toward the central source. There is a clear contradiction with the UV observations of the source since continuum fluorescence also affects the lines Ne VIII λ774 and O VI λ1035, and the two are calculated to be much stronger than the proposed 88 Å lines and also Lyα. This would lead to a UV spectrum never observed in AGNs. Thus, from the point of view of the observed 70–100 Å equivalent widths and the relative line intensities, the proposed identifications of the *EUVE* 88 Å feature are questionable.

4.4. *Ultraviolet Absorption Lines*

Intrinsic absorption systems are often observed in the *IUE* spectra of Seyfert 1 galaxies and low-redshift quasars (Ulrich 1988). About one in 10 Seyfert 1 galaxies shows C IV λ1549 in absorption, and the actual number is likely to be larger because of the limited resolution and S/N of *IUE*.

Several recent papers (Mathur et al. 1994; Mathur 1994; Mathur et al. 1995; Kriss et al. 1996a) have addressed the possible association of such systems with the warm X-ray absorbers. In two quasars, 3C 351 (Mathur et al. 1994) and 3C 212 (Mathur 1994), and in one Seyfert 1 galaxy, NGC 5548 (Mathur et al. 1995), there seems to be good agreement between the observed UV and X-ray absorption, and the authors argued that all absorption was due to the same physical component. In another Seyfert 1 galaxy, NGC 3516 (Kolman et al. 1993; Kriss et al. 1996a), the situation is more complex and probably time-dependent. According to Kriss et al. (1996a), the observed C IV λ1549, N V λ1240, and O VI λ1035 absorption lines are inconsistent with the parameters of the strongest X-ray absorber, as observed simultaneously by *ASCA*. These authors concluded that there are several UV-absorbing components and that the strongest absorption lines come from gas that is considerably more neutral than the observed X-ray component.

To address this issue in a systematic way, we have calculated C^{+3}, N^{+4}, O^{+5}, and Ne^{+7} column densities for the entire parameter space considered here. The results are shown in Figure 11 as column densities of the absorbing ions and as line equivalent widths for a specific Doppler parameter of 100 km s^{-1}, similar to that observed in several well-studied cases. The calculations pertain only to the continua discussed here (Fig. 1), and individual objects should be investigated with their observed continuum since the shape of the 50–150 eV continuum may differ from ours.

Given the chosen continuum, it is evident that a significant EW(C IV λ1549) can only be attained for large ($>10^{22}$ cm^{-2}) column densities. In particular, the small X-ray column deduced for NGC 5548 (Mathur et al. 1995 and references therein) of 3.8×10^{21} cm^{-2} makes it difficult to explain the observed C IV λ1549 equivalent width in this source. Of greater importance is the consistency check between C IV λ1549, N V λ1240, and O VI λ1035. Because of the increasing ionization potential, and despite the smaller nitrogen abundance, the absorption equivalent width of O VI λ1035 is always the largest, and that of N V λ1240 is almost always larger than EW(C IV λ1549). This presents a serious problem for NGC 5548 and perhaps other sources. The definitive test is the equivalent width of O VI λ1035, which is calculated to be significant in almost all cases of warm X-ray absorbers. This could be tested against the handful of Hopkins Ultraviolet Telescope Seyfert 1 obser-

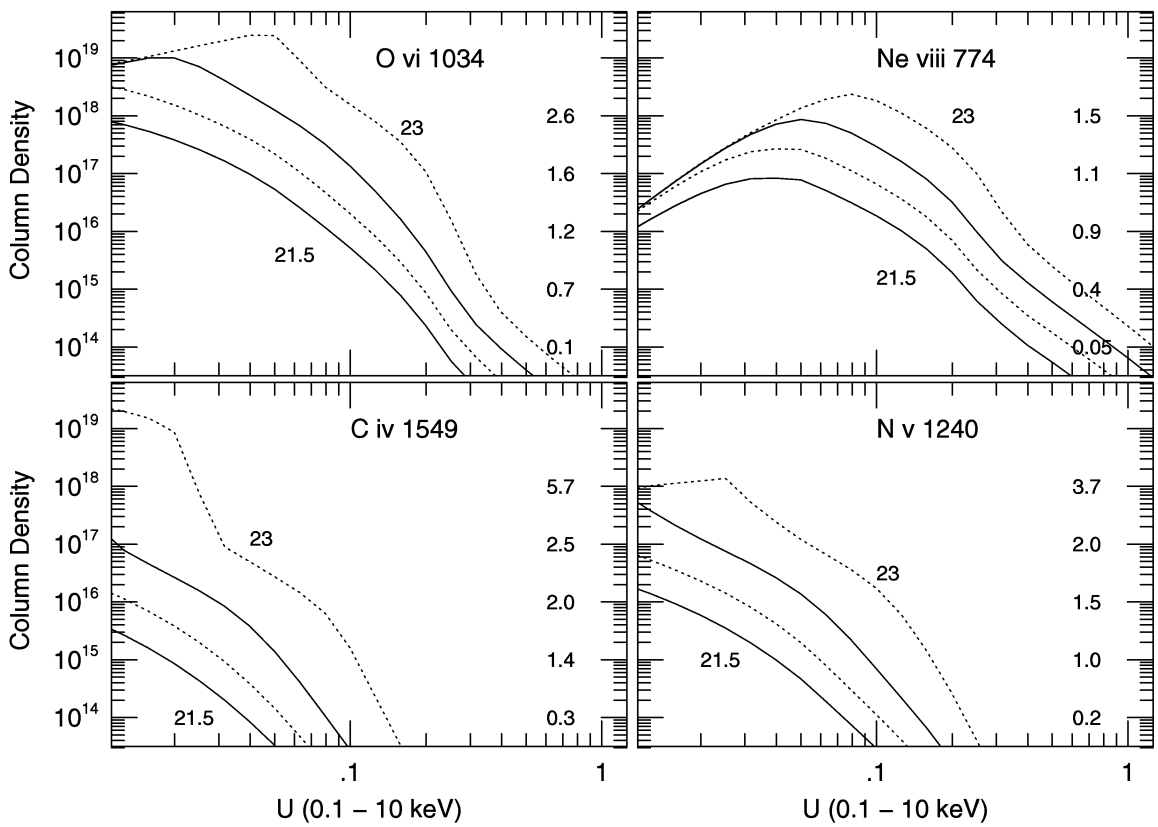

FIG. 11.—Calculated column densities for C^{+3}, N^{+4}, O^{+5}, and Ne^{+7} and corresponding absorption equivalent widths of strong UV lines. The gas density is 10^{11} cm^{-3}, and the four curves represent total (hydrogen) column densities of $10^{21.5}$, 10^{22}, $10^{22.5}$, and 10^{23} cm^{-2}, as marked. Numbers on the right-hand side are calculated absorption equivalent widths (in angstroms), assuming thermal profiles with a Doppler parameter of 100 km s^{-1}.

vations and the numerous observations of $z > 0.1$ quasars, especially those suspected to show warm X-ray absorption.

4.5. *Locations and Properties of Ionized Absorbers*

A very interesting question of AGN X-ray research is the location and properties of the ionized absorbing gas. Paper I focused on nearby gas, as close as or even closer than the BLR. Many of the models shown in the present work, and the chosen fiducial density of 10^{11} cm^{-3}, pertain to this possibility. Here we extend the discussion to include other locations, with emphasis on a new idea that unifies the "classical" BLR and the X-ray absorber. The discussion is based on the following estimated density of the warm absorbing gas:

$$N_{\rm WA} \simeq 3 \times 10^4 L_{44} R_{\rm pc}^{-2} \ {\rm cm}^{-3} , \qquad (6)$$

obtained by scaling to the typical ionization parameter of the 10^{10} cm^{-3} BLR gas, and it assumes an approximate BLR size of $R_{\rm BLR} \simeq 0.01 L_{44}^{1/2}$ pc, where L_{44} is the ionizing luminosity in units of 10^{44} ergs s^{-1}.

Spectral fittings of absorbed X-ray spectra are insensitive to the density and hence the location of the absorbing gas. They are sensitive to the covering fraction and, to some extent, to the gas velocity. Assuming a general decrease of density as a function of distance from the center, we identify two major differences between compact and extended absorbers, the recombination time and the amount of absorbing gas (related also to the physical size of the absorber). A search for time-variable absorbing features will provide a measurement of the recombination time and will help to identify the location of the gas. This has been extensively discussed in the literature, most recently by Reynolds et al. (1995) and Mathur et al. (1995). Emission-line variations, in response to the varying X-ray continuum, have been suggested as another means of locating the X-ray absorber (George et al. 1995). This is currently under investigation. As for the second difference, the larger inferred mass of extended absorbing gas has little implication to X-ray spectral fittings but is crucial for the modeling of the nucleus. For example, a detection of expansion velocity will indicate a gas reservoir near the center. Such streaming gas, if of low enough density, contains most of the mass of the nucleus outside the black hole and the central accretion disk.

Given the limited information on the absorbing gas density, column density, ionization, and covering fraction, we suggest the following "evaporating cloud model" for AGNs: The model assumes a clumpy BLR with a covering factor of order 0.1, $n_{\rm H} \sim 10^{10}$ cm^{-3}, and approximately spherical distribution. The "clouds" are either bloated stars with extended winds (Alexander & Netzer 1994, 1996) or seeds of high density that lose mass to the intercloud medium. For bloated stars, the winds are attached to the star up to a radius of order 10^{14} cm, where the wind density is a few times 10^9 cm^{-3}. This outer radius is determined by tidal forces and Comptonization (Alexander & Netzer 1996). The seeds may be smaller, with density and dimensions similar to what is customarily assumed for BLR clouds. The flow produces lower density, higher ionization gas of large covering fraction. A stable situation may involve wind material filling almost all space between clouds and decreasing in density as it moves away from the seeds, reaching a density of a few times 10^8 cm^{-3}. The decreasing density results in an increasing level of ionization, corresponding to increase in $U_{\rm X}$ by an order of magnitude at the point where the gas detaches itself from the clouds, i.e., some 10–40 times the ionization parameter of the BLR gas. At such $U_{\rm X}$, the electron temperature is still below $T_{\rm max}$, discussed in § 2. The dominant stages of ionization of oxygen are O^{+6}–O^{+8}, and the column density is comparable to the column density of the BLR clouds (the outer layers of the bloated star).

General considerations suggest that the intercloud, high-ionization gas, which is exposed to the full radiation of the central source, is accelerated outward and that the density and column density decrease with distance. At an expansion velocity of a few hundred km s^{-1}, the density is of the order of 10^8 cm^{-3} and the ionization parameter is a few times larger than the previously mentioned value, i.e., about 50 times that in the edge of the clouds. At this value of $U_{\rm X}$, the gas temperature is close to $T_{\rm max}$, and further reduction in density causes it to become unstable and disappear from direct view.

A full solution, combining the gas motion and dynamics with the mass loss from the seeds, is beyond the scope of this paper. The stability of the cloud must be addressed, as well as the total Compton depth of the medium. There is yet no independent evidence for the outward motion of the X-ray–absorbing gas (except for the consistency argument involving the UV absorption lines), and there are other uncertainties. We note, however, the similarity of the mass-loss rate from bloated stars (Alexander & Netzer 1996) and that inferred from the velocity of the UV absorption systems. We also note that the level of ionization of the warm X-ray gas, as observed in many AGNs, and its covering fraction are consistent with the density, column density, and covering fraction assumed in this model. Finally, the ionized gas pressure is comparable to the BLR gas pressure. If proved correct, the model can account for all the observed UV and X-ray components: broad emission lines, narrow blueshifted absorption lines from gas outside of the BLR, and X-ray absorption and emission. A highly simplified picture demonstrating this idea is shown in Figure 12.

4.6. *Open Questions*

Several issues discussed in this paper are still observationally or theoretically unknown. The partial list below could serve as a starting point for further study.

1. How common are warm absorbers in AGNs? Are they less frequent in high-luminosity AGNs?
2. How common are UV absorption lines? Are they detected in *all cases* in which a large column density of X-ray gas is present? If not, why?
3. Can the location and density of the warm X-ray–absorbing gas be deduced from reverberation mapping of X-ray lines?
4. How strong are the iron L-shell lines? Can they influence the determination of absorption-feature energies?
5. How stable is the warm absorbing gas, and what is the effect of expansion cooling on the derived temperature and level of ionization?
6. What is the covering fraction of the warm absorbing gas? Is it a function of distance from the center?
7. How viable is the "evaporating cloud model"? Are the predicted mass loss, column density, and covering fraction consistent with the observations?
8. Are there several distinct warm-absorber components? This would require the calculation of different

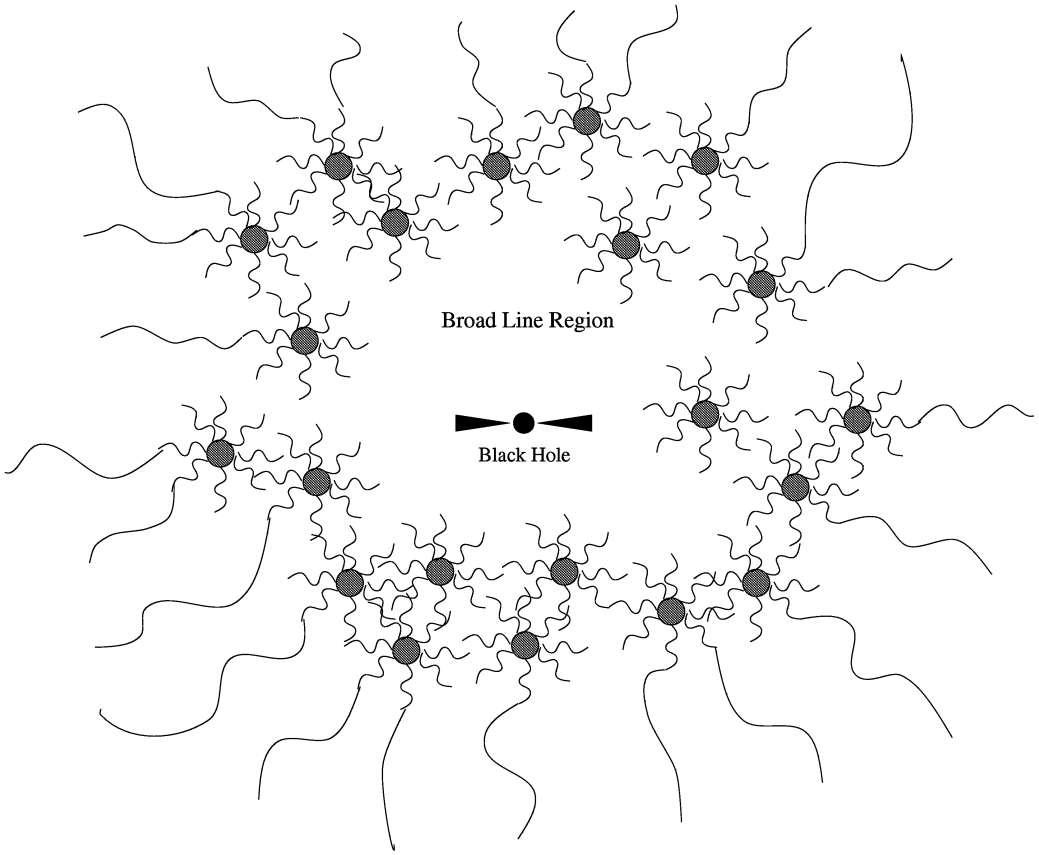

FIG. 12.—Simplified composite model combining mass loss from BLR clouds ("seeds" or bloated stars) with the resulting outflowing intercloud medium, which is responsible for the UV and X-ray absorption.

geometries in which different lines of sight combine emission and absorption in different proportions.

5. CONCLUSIONS

We have investigated the most important physical processes in X-ray–photoionized gases and shown calculated line intensities and equivalent widths over a large range of density, column density, and ionization parameter. We found that, in unobscured AGNs, the strongest 0.1–10 keV lines will show as small (5–50 eV) equivalent width emission features. Obscured AGNs, like Seyfert 2's, are expected to show much stronger lines. We have investigated the stability and temperature of the X-ray–absorbing gas and find that the gas is thermally stable up to a temperatures of about 2×10^5 K. Continuum fluorescence of X-ray lines is not significant for the column density and level of ionization thought to be typical of warm absorbers in AGNs. The X-ray–ionized gas is expected to produce some strong far-UV emission lines, and its properties are similar to those deduced for several UV-absorbing systems. Combining all known nuclear components in AGNs, a model has emerged in which the X-ray–absorbing gas is just outside the BLR with a typical density of a few times 10^8 cm^{-3}.

It is a pleasure to acknowledge informative and helpful discussions with Ian George, Jane Turner, Tim Kallman, Richard Mushotzky, Paul Nandra, Gary Ferland, Amiel Sterberg, Ari Laor, and Tal Alexander. I am grateful to Duen Liedahl, Nancy Brickhouse, Dima Verner, and Ken Dere for providing most useful atomic data and for allowing me to use some of their unpublished calculations. This research is supported by USRA, an ADP NASA grant (NAG5-1813), the Jack Adler Chair of Extragalactic Astronomy, and a special grant from the Israel Science Foundation.

APPENDIX

General descriptions of ION can be found in Paper I, in Netzer et al. (1994), and in references cited therein. Below we provide some more information pertaining to the present work.

A1. H-LIKE AND He-LIKE LINES

All H-like ions, except for hydrogen and He^+, are treated as five-level systems plus a continuum. The $2s$ and $2p$ levels are treated individually, and the other levels are assumed to be collisionally mixed. The main source for the $2s$–$2p$ collisions is Zygelman & Dalgarno (1987). Other collisional rates are obtained from references cited in Callaway (1994). Transfer in all lines is included with the standard escape-probability formalism.

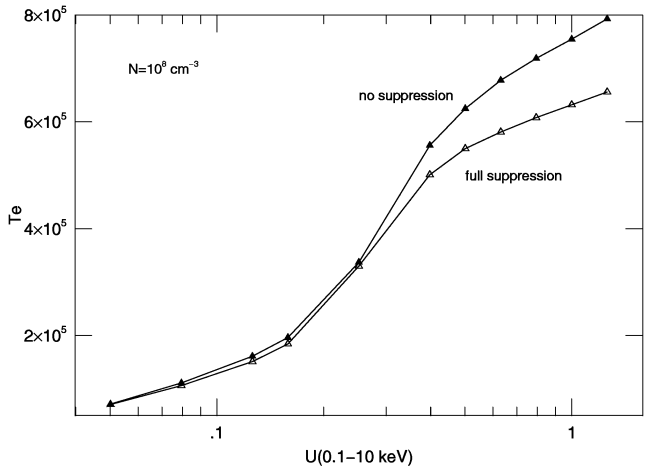

FIG. 13.—Temperature vs. ionization parameter for two extreme assumptions about the density dependence of the dielectronic recombination rates. The suppression is according to eq. (A1), and all models calculated in this paper fall between the lines, closer to the full-suppression curve.

He-like ions, except for He I, are treated as seven-level systems, including the levels 1 ^1S, 2 ^1S, 2 ^1P, 2 ^3S, and 2 ^3P (three levels). Collisional rates are based on the references in Dubau (1994) and do not include collisions with protons (e.g., Mewe & Schrijver 1978). All optical depths are treated with the local escape probability, and all emitted photons are lumped, in the final stage, into one representing transition.

A2. PHOTOIONIZATION AND RECOMBINATION

The present calculations do not make use of the new Opacity Project photoionization rates (Verner et al. 1996). This is not very important since the inner-shell cross sections, and the cross sections of highly ionized ions, are not likely to change by much.

Radiative recombination rates are based on the photoionization cross sections. Dielectronic recombination at low temperature is not very important, but the density-sensitive high-temperature dielectronic rates can dominate the recombination of many species. The density-dependent coefficients for those were not available, and we have adopted a simplified, uniform-density suppression factor, S_p, for all ions at all densities above 10^5 cm^{-3}. This has the form

$$S_p = \max\,[S_{p,\max}, 1.818(1 - 0.09 \log N_e)]\,, \qquad \text{(A1)}$$

where $S_{p,\max}$ is adjustable. We have investigated the dependence on this assumption by calculating the gas temperature, over a large range of density and U_X, with several chosen values of $S_{p,\max}$. An example showing this behavior for $n_H = 10^8$ cm^{-3} is given in Figure 13. As seen in the diagram, the gas temperature is indeed sensitive to the dielectronic recombination rate at large U_X. The value of $S_{p,\max}$ chosen for all calculations in this paper is 0.1, which results in temperatures close to the full-suppression curve shown in the diagram. This density sensitivity can explain part of the line intensity behavior shown in Figure 8.

Three-body recombination is important at all densities exceeding $\sim 10^{11}$ cm^{-3}. Its relative contribution to the total rate is a function of temperature and charge of the recombining ion. The calculations assume that all high-temperature dielectronic recombination and three-body recombination are to high energy levels. Thus the effective recombination coefficients of most lines, and the ground-level recombination, were computed with an enhancement factor, taking into account the extra recombination, on top of the radiative recombination contribution.

Finally, we have included additional recombination lines, on top of the already mentioned H-like and He-like lines. There are between three and five lines per lithium-like ion, three lines for each of the beryllium-like ions, and several Fe L lines. For the Li-like and Be-like ions, we do not have accurate effective recombination coefficients, and the calculated intensities are rather uncertain. More accurate data were available for many iron L-shell lines (D. Liehdal, 1995, private communication). The present calculations include only the three to five strongest lines per ion for Fe XVII–XXIV.

REFERENCES

Alexander, T., & Netzer, H. 1994, MNRAS, 270, 781
———. 1996, MNRAS, in press
Band, D. L., Klein, R. I., Castor, J. I., & Nash, J. K. 1990, ApJ, 362, 90
Callaway, J. 1994, At. Data Nucl. Data Tables, 57, 9
Dubau, J. 1994, At. Data Nucl. Data Tables, 57, 21
Elitzur, M., & Netzer, H. 1985, ApJ, 291, 464
Fabian, A. C., et al. 1994, PASJ, 46, L59
Ferland, G. J., & Rees, M. J. 1988, ApJ, 332, 141
Fiore, F., Elvis, M., Mathur, S., Wilkes, B. J., & McDowell, J. C. 1993, ApJ, 415, 129
George, I. M., & Fabian, A. C. 1991, MNRAS, 249, 352
George, I. M., Turner, T. J., & Netzer, H. 1995, ApJ, 438, L67
Halpern, J. 1984, ApJ, 281, 90
Hamann, F., Shields, J. C., Ferland, G. J., & Korista, K. T. 1995a, ApJ, 454, 688
Hamann, F., Zou, L., & Tytler, D. 1995b, ApJ, 444, L69
Kaastra, J. S., Roos, N., & Mewe, R. 1995, A&A, 300, 25
Kolman, M., Halpern, J. P., Martin, C., Awaki, H., & Koyama, K. 1993, ApJ, 403, 592
Kriss, G. A., Espey, B. A., Krolik, J. H., Tsvetanov, Z., Zheng, W., & Davidson, A. F. 1996a, ApJ, 467, 622
Kriss, G. A., et al. 1996b, ApJ, 467, 629
Krolik, J. H., & Kallman, T. 1984, ApJ, 286, 355
Krolik, J. H., & Kriss, G. A. 1995, ApJ, 447, 512 (KK95)
Krolik, J. H., McKee, C. F., & Tarter, C. B. 1981, ApJ, 249, 422
Laor, A. 1990, MNRAS, 246, 369
Liedahl, D. A., Osterheld, A. L., & Williams, H. G. 1995, ApJ, 438, L115
Mathur, S. 1994, ApJ, 431, L75
Mathur, S., Elvis, M., & Wilkes, B. 1995, ApJ, 452, 230
Mathur, S., Wilkes, B., Elvis, M., & Fiore, F. 1994, ApJ, 434, 493

Marshall, F. E., et al. 1993, ApJ, 405, 168
Mewe, R., & Schrijver, J. 1978, A&A, 65, 99
Nandra, K., & Pounds, K. 1992, Nature, 359, 215
———. 1994, MNRAS, 268, 405
Netzer, H. 1976, MNRAS, 177, 473
———. 1990, in Active Galactic Nuclei, ed. T. Courvoisier & M. Mayor (Berlin: Springer), 57
———. 1993, ApJ, 411, 594 (Paper I)
Netzer, H., Turner, T. J., & George, I. M. 1994, ApJ, 435, 106
Pan, H., Stewart, G. C., & Pounds, K. A. 1990, MNRAS, 242, 177
Reynolds, C. S., Fabian, A. C., Nandra, K., Inoue, H., Kunieda, H., & Iwasawa, K. 1995, MNRAS, 277, 901
Shields, J. C., Ferland, G. J., & Peterson, B. M. 1995, ApJ 441, 507
Turner, T. J., Netzer, H., & George, I. M. 1996, ApJ, 463, 134
Turner, T. J., & Pounds, K. A. 1989, MNRAS, 240, 833
Ulrich, M. H. 1988, MNRAS, 230, 121
Verner, D. A., Ferland, G. J., Korista, K. T., & Yakovlev, D. G. 1996, ApJ, 465, 487
Ward, M., Elvis, M., Fabbiano, G., Carleton, N. P., Willner, S. P., & Lawrence, A. 1987, ApJ, 315, 74
Wills, B. J., Netzer, H., & Wills, D. 1985, ApJ, 288, 94
Yaqoob, T., et al. 1996, ApJ, in press
Yaqoob, T., & Warwick, R. S. 1991, MNRAS, 248, 773
Życki, P. T., Krolik, J. H., Zdziarski, A. A., & Kallman, T. R. 1994, ApJ, 437, 597
Zygelman, B., & Dalgarno, A. 1987, Phys. Rev. A, 35, 4085

Note added in proof.—After this paper was accepted for publication, we received a paper by T. R. Kallman, D. Liedahl, A. Osterheld, W. Goldstein, & S. Kahn (ApJ, 465, 994 [1996]). The treatment of the Fe L spectrum in this paper is much more complete than that in the present work, and many more lines are included. However, the paper addresses only the optically thin situation and cannot, therefore, be applied for most of the models shown here.